Energy Conversion

Deutsche Ausgabe: DOI: 10.1002/ange.201505339
Internationale Ausgabe: DOI: 10.1002/anie.201505339

Dissolution Engineering of Platinum Alloy Counter Electrodes in Dye-Sensitized Solar Cells

Qunwei Tang, Huihui Zhang, Yuanyuan Meng, Benlin He, and Liangmin Yu**

Abstract: *The dissolution of platinum (Pt) has been one of the heart issues in developing advanced dye-sensitized solar cells (DSSCs). We present here the experimental realization of stable counter-electrode (CE) electrocatalysts by alloying Pt with transition metals for enhanced dissolution resistance to state-of-the-art iodide/triiodide (I^-/I_3^-) redox electrolyte. Our focus is placed on the systematic studies of dissolution engineering for $PtM_{0.05}$ (M = Ni, Co, Fe, Pd, Mo, Cu, Cr, and Au) alloy CE electrocatalysts along with mechanism analysis from thermodynamical aspects, yielding more negative Gibbs free energies for the dissolution reactions of transition metals. The competitive reactions between transition metals with iodide species (I_3^-, I_2) could protect the Pt atoms from being dissolved by redox electrolyte and therefore remain the high catalytic activity of the Pt electrode.*

The dye-sensitized solar cell (DSSC)[1,2] is considered as a potentially cost-effective alternative to commonly used silicon solar cells. Precious platinum (Pt) has been the most preferred counter electrode (CE) electrocatalyst for DSSCs because of its high electron-conducting ability, electrocatalytic activity toward I_3^- reduction reaction at the CE/electrolyte interface, high light-reflecting properties, and charge-transfer capability to liquid electrolyte by increasing the surface-to-volume ratio.[3,4]

The I_3^- reduction reaction is of utmost significance in the state-of-the-art photoelectrochemical conversion of liquid-junction DSSCs. The sluggish kinetics of the I_3^- reduction reaction demands a high loading of Pt electrocatalysts,[5] which unfavorably increases the costs of DSSCs. At this juncture, the catalytic efficiency of CE electrocatalysts for the I_3^- reduction reaction is required to be substantially improved so that the dependency on noble Pt can be significantly weakened or fully eliminated. On the other hand, the unsatisfactory long-term stability of Pt electrocatalysts suffering from persistent corrosion on exposure to I^-/I_3^- redox electrolyte remains a major obstacle. Nevertheless, our ability to control the reduction of fabrication costs and to improve the catalytic activity is still limited to combine Pt with carbonaceous materials or conductive polymers, or completely replace Pt by single-metal sulfides, nitrides or carbides or their composites. The main issues refer to structural alteration and collapse under electrochemical conditions. Therefore, we have to pay our attention to metallic CE electrocatalysts.[6–10] Recently, we have reported the successful realization of alloyed CE electrocatalysts by alloying Pt with transition metals,[6] transition metal with transition metal,[7] or transition metal with non-metal.[8] In the current work, we mainly present the experimental realization of alloyed $PtM_{0.05}$ (M = Ni, Co, Fe, Pd, Mo, Cu, and Cr) CE electrocatalysts with a dissolution resistance superior to a pristine Pt electrode, and launch a theoretical perception for protecting Pt from dissolution and for remaining a persistent catalytic activity.

Figure S1 represent the SEM images of as-prepared electrocatalysts, depicting an uncompacted structure. These images emphasize the surface-to-volume ratio and the higher catalytic activity of these electrocatalysts, for example, for the I_3^- reduction reaction. As shown in Figure S9e, pristine Pt before dissolution exhibits two energy bands at 71.6 and 74.8 eV, corresponding to $Pt4f_{7/2}$ and $Pt4f_{5/2}$ core electrons, respectively. The two peak positions and the binding energy difference ($\Delta E = 3.2$ eV) between the doublet belong to metallic Pt^0. When alloyed with transition metals, the peak for $Pt4f_{7/2}$ has a downshift of 0.5, 0.6, 0.6, 0.3, 0.7, 0.5, and 0.5 eV for $PtNi_{0.05}$, $PtCo_{0.05}$, $PtFe_{0.05}$, $PtPd_{0.05}$, $PtMo_{0.05}$, $PtCu_{0.05}$, and $PtCr_{0.05}$ (Figure S2a), respectively. The downshift of the binding energies for the $Pt4f_{7/2}$ electrons may be ascribed to the electronic interactions between the Pt and M atomic orbitals, leading to (or partial) electron transfer from M to Pt.[11] This conclusion also demonstrates that the ligaments of CE electrocatalysts are composed of alloyed metallic Pt and M. To reveal how M does interact with Pt and impact the electronic structure of Pt, we compare the electronegativities and lattice constants of the employed transition metals; they are 1.92/3.53 Å (Ni), 1.88/2.51 Å (Co), 1.83/2.87 Å (Fe), 2.20/3.89 Å (Pd), 2.16/3.15 Å (Mo), 1.90/3.61 Å (Cu), and 1.66/2.88 Å (Cr), which are lower than 2.28/3.92 Å for metallic Pt. In this fashion, the deviation of an electron from M to Pt is observed in the alloyed $PtM_{0.05}$, which renders the Pt surface and its catalytic sites electronically "hotter" in comparison with pristine Pt.[12] However, the M atoms with a lower lattice constant may enter the face-centered cubic Pt lattice to tune the binding strength between Pt and I, and to create many actives for electrolyte adsorption.[13] Moreover, the chemical formulae of the CE electrocatalysts are determined to be $PtNi_{0.063}$, $PtCo_{0.052}$, $PtFe_{0.071}$, $PtPd_{0.048}$, $PtMo_{0.050}$, $PtCu_{0.051}$, and $PtCr_{0.043}$ by calculating the surface atomic ratios in the XPS spectra (Figure S2a),[14]

[*] Prof. Q. Tang, H. Zhang, Y. Meng, Dr. B. He, Prof. L. Yu
Key Laboratory of Marine Chemistry and Technology
Ministry of Education, Ocean University of China
Qingdao Collaborative Innovation Center of Marine Science and Technology, Ocean University of China, Qingdao 266100 (P.R. China)
E-mail: tangqunwei@ouc.edu.cn
yuyan@ouc.edu.cn
Prof. Q. Tang, H. Zhang, Y. Meng, Dr. B. He
Institute of Materials Science and Engineering
Ocean University of China, Qingdao 266100 (P.R. China)

Supporting information for this article is available on the WWW under http://dx.doi.org/10.1002/anie.201505339.

respectively. The measured atomic ratios are similar to their stoichiometries, therefore, the chemical formulas of the binary Pt$M_{0.05}$ alloys can be expressed according to the stoichiometric ratios.

Figure 1 a represents photocurrent density–voltage (J–V) curves for the DSSCs under air mass 1.5 global sunlight, and the photovoltaic parameters are summarized in Table S1. A conversion efficiency (η) of 7.10 % is determined on the DSSC with the pristine Pt-based CE, and this value is enhanced to 7.93, 7.75, 7.54, 7.48, 7.28, and 7.17 % by alloying Pt with Ni, Co, Fe, Pd, Mo, Cu, and Cr, respectively. From a small standard deviation (± 5 %), as shown in Figure S3, we infer that the DSSCs with promising photovoltaic performances and high reproducibility can be realized using the method reported here. Moreover, the cell efficiency can be further enhanced by optimizing the chemical compositions (Figure S4).

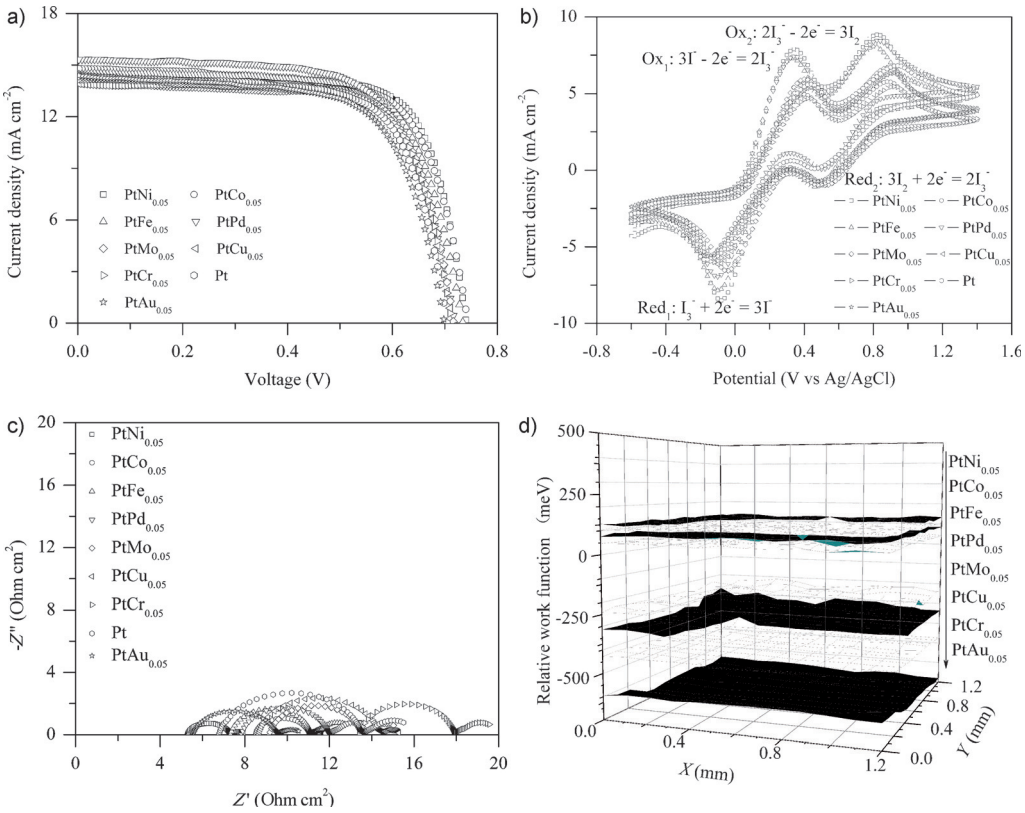

Figure 1. a) Characteristic J–V curves for the DSSCs with various CEs. b) CV curves of various CEs for the I^-/I_3^- redox electrolyte recorded at a scan rate of 50 mV s^{-1}. c) Nyquist EIS plots for the symmetric dummy cells from two identical CEs. d) Relative work functions of various CEs.

The electrocatalytic activities of the Pt$M_{0.05}$ CE toward the I_3^- reduction reaction are evaluated by cyclic voltammetry (CV) characterization. As shown in Figure 1 b, two pairs of redox peaks corresponding to Red_1/Ox_1 ($I_3^- + 2e^- = 3I^-$/ $3I^- - 2e^- = I_3^-$) and Red_2/Ox_2 ($3I_2 + 2e^- = 2I_3^-$/$2I_3^- - 2e^- = 3I_2$) are detected in each CV curve. The main function of a CE is to reduce I_3^- to I^- ions at the CE/electrolyte interface after undergoing a two-electron process, therefore, characteristic performances for the Red_1 peak, such as the peak current density of Red_1 (J_{Red1}) and the peak-to-peak separation (E_{pp}), are always used to evaluate the catalytic activity. As summarized in Table S2, the synthetical catalytic activities follow the order $PtNi_{0.05} > PtCo_{0.05} > PtFe_{0.05} > PtPd_{0.05} > PtMo_{0.05} > PtCu_{0.05} > PtCr_{0.05} > Pt$ during the diffusion-controlled process of the I^-/I_3^- couple at the CE/electrolyte interfaces (Figure S5).[15] From Figure 1 c and Table S2, the charge-transfer resistance (R_{ct}) values follow the order $PtNi_{0.05}$ (1.29 Ω cm^2) < $PtCo_{0.05}$ (1.46 Ω cm^2) < $PtFe_{0.05}$ (3.35 Ω cm^2) < $PtPd_{0.05}$ (3.74 Ω cm^2) < $PtMo_{0.05}$ (3.83 Ω cm^2) < $PtCu_{0.05}$ (3.93 Ω cm^2) < $PtCr_{0.05}$ (4.12 Ω cm^2) < Pt (6.59 Ω cm^2). A low R_{ct} at the CE/electrolyte interface means a rapid participation in the I_3^- reduction reaction ($I_3^- + 2e^- = 3I^-$), therefore the electron lifetime (τ) for the I_3^- reduction [$\tau = 1/(2\pi f_{max})$, f_{max} is the peak frequency in the Bode electrochemical impedance spectroscopy (EIS) plots corresponding to charge transfer at the CE/electrolyte interface, as shown in Figure S6] can be used to evaluate the reaction rate, they are 42.3, 48.8, 53.4, 58.5, 70.1, 84.0, 87.9, and 105.5 μs for $PtNi_{0.05}$, $PtCo_{0.05}$, $PtFe_{0.05}$, $PtPd_{0.05}$, $PtMo_{0.05}$, $PtCu_{0.05}$, $PtCr_{0.05}$, and Pt, respectively. This result is in agreement with CV characterization. To demonstrate why and how the alloy species do tune the catalytic activity and charge-transfer ability of a CE electrocatalyst, we have measured work functions of the CEs [work function = −(5.1−relative work function)]. As shown in Figure 1 d, the CE of $PtNi_{0.05}$ has a work function of −4.990 eV which matches better the potential of the I^-/I_3^- redox reactions (−4.9 eV) compared with −4.993, −5.048, −5.050, −5.374, −5.432, and −5.543 eV for $PtCo_{0.05}$, $PtFe_{0.05}$, $PtPd_{0.05}$, $PtMo_{0.05}$, $PtCu_{0.05}$, and $PtCr_{0.05}$,[16] respectively. The mimimum work function for $PtNi_{0.05}$ is attributed to more electron transfer from Ni to Pt, leading to a weak binding energy of the electrons. Therefore, these weakly bound electrons are more favorable to participating in the I_3^- reduction at the NiM surface. Notably, R_{ct} can be determined by the difference between the redox potential for the I^-/I_3^- pairs and the work function of a CE electrocatalyst (Scheme 1 a), and these differences are 0.090, 0.093, 0.148, 0.150, 0.474, 0.532, 0.643, and 0.900 eV for $PtCo_{0.05}$, $PtFe_{0.05}$, $PtPd_{0.05}$,

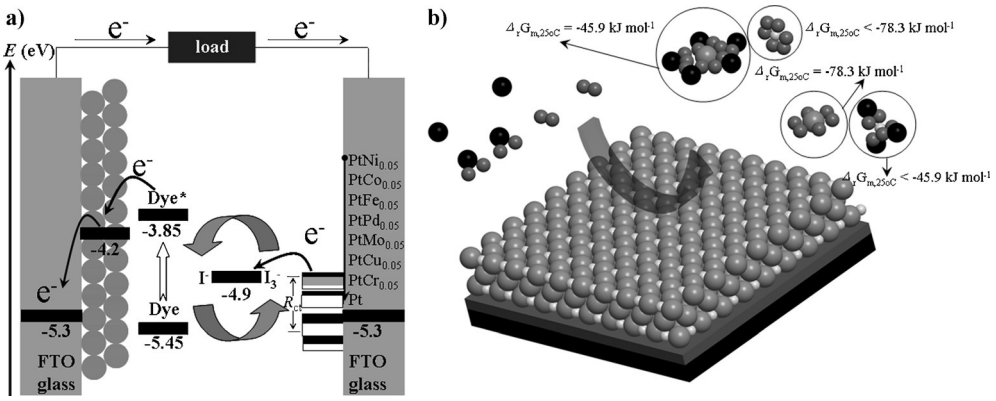

Scheme 1. Schematic diagram of a) electron transfer at the CE/electrolyte interface and b) Pt$M_{0.05}$ alloy electrocatalysts suffering from I^-/I_3^- electrolyte dissolution.

$PtMo_{0.05}$, $PtCu_{0.05}$, $PtCr_{0.05}$, and pristine Pt, respectively. A weak energy drop means a weaker demand for energy demand and therefore a lower R_{ct} for the electron transfer from the electrocatalyst to the redox electrolyte. The results from EIS analysis are consistent with the work function characterizations. Moreover, the measured work function, defined as the minimum energy necessary to remove an electron from a given solid surface to a point immediately outside the surface, can provide an evaluation for the energy of surface electrons that interact with I_3^- adsorbates.[17] Figure S7 illustrates the idea of the work function as a descriptor on the alloys of the electrochemical I_3^- evolution reaction. There appears to be an approximately linear correction between the work function and the electrocatalytic activity of the corresponding Pt$M_{0.05}$ electrocatalysts toward I_3^- reduction. The decrease of the work function from $PtNi_{0.05}$ to Pt indicates that charges facilitate to transfer from the adsorbed I_3^- ions to the Pt$M_{0.05}$ electrocatalysts. The adsorption energy of I_3^- ions by CE electrocatalyst decreases and the Pt–I distance increases.[18]

Pt dissolution in the I^-/I_3^- redox electrolyte has been an unsettled issue since the birth of DSSCs using mesoscopic semiconductor oxide layers. As depicted in Scheme 1b, both Pt and *M* atoms suffer from electrolyte attack (dissolution in electrolyte by I_3^- and I_2 species). We have carried out thermodynamic calculations with regard to the formation of these compounds at 25 °C. The possible dissolution reactions and corresponding Gibbs free energy ($\Delta_r G_m$) are summarized in Table S3. Regardless of the thermodynamically unfavored reactions with I^- (The calculated $\Delta_r G_m$ values for $Pt(s) + I_3^-(aq) + I^-(aq) = PtI_4^{2-}(aq)$ and $M(s) + I_3^-(aq) + I^-(aq) = MI_4^{2-}(aq)$ are positive.), all the dissolution reactions have highly negative $\Delta_r G_m$ values, suggesting that the dissolution of Pt or *M* by I_3^- and I_2 is a thermodynamically spontaneous process. Notably, the $\Delta_r G_m$ for chemical reactions between *M* and I_3^- or I_2 are more negative relative to that of metallic Pt. The extent of the total dissolution reaction of Pt$M_{0.05}$ alloy electrocatalyst is determined by competitive reactions between Pt and halides or between *M* and halides. Figure 2 shows the stacking 100-cycle CV curves in liquid electrolyte recorded at a scan rate of 50 mV s^{-1} as well as the repeated 100-cycle Nyquist and Bode plots of the symmetric dummy cells. By plotting the extracted J_{red1}, R_{ct}, and τ values at the CE/electrolyte interface, as shown in Table S4, we can evidently find that the J_{Red1}, R_{ct}, and τ for the pristine Pt electrode are reduced by 0.031%, increased by 0.297%, and increased by 0.153%, respectively. As described previously, the reduced J_{Red1}, and increased R_{ct} and τ triply mean a reduction in the catalytic activity. When alloyed with transition metals, the catalytic activity has a slight increase or at least remains nearly unchanged after 100 cycles even at high transition-metal dosage (Figure S10 and Table S5). These results show that the competitive reaction between transition metals and I_3^- (and I_2) reduces the dissolution of Pt species and therefore enhances the stability in I^-/I_3^- electrolyte.

Comparing the surface topographies of Pt and $PtNi_{0.05}$ before and after 20 cycles at a scan rate of 50 mV s^{-1} by scanning the I^-/I_3^- redox electrolyte, as shown in Figure S1a, b and Figure S9a, b, one can discover that the multiple catalysis of Pt or $PtNi_{0.05}$ toward the I^-/I_3^- redox couple leads to dissolution and therefore to a looser structure on an fluorine-doped tin oxide (FTO) glass. As has been above-mentioned, the real chemical composition of $PtNi_{0.05}$ is $PtNi_{0.063}$ before dissolution (Figure S2a), while it is determined to be $PtNi_{0.026}$ after 20 CV cycles scanned by X-ray photoelectron spectroscopy (XPS; Figure S9e). The consumption of the Ni species is attributed to the thermodynamically favored reaction between Ni and I_3^-/I_2. This distinction is cross-checked by alloying Pt with a metal having more positive $\Delta_r G_m$ values when reacted with halides. As shown in Figure S9c, d, a similar loose structure is observed after dissolution in redox electrolyte, while the chemical compositions are determined to be $PtAu_{0.024}$ and $PtAu_{0.056}$ before and after scanning in I^-/I_3^- electrolyte, respectively. This enhancement in Au content refers to a better dissolution of Pt by liquid electrolyte arising from more thermodynamically favored reactions, which can be further confirmed by the markedly reduced J_{Red1}, and significantly enhanced R_{ct} and τ in Figure 2 and Table S4. This conclusion is also applicable in explaining the poor catalytic activity and photovoltaic behavior of $PtAu_{0.05}$ in a DSSC (Figure S2b and Figure 1).

In summary, the alloying of Pt with transition metals such as Ni, Co, Fe, Pd, Mo, Cu, or Cr is shown to be a promising strategy in enhancing the catalytic activities of CE electrocatalysts for liquid-junction DSSCs, attributing to electron-enriched Pt surfaces and good matching of work functions with the redox potential of the I^-/I_3^- pair. More importantly, the preliminary results reveal that the Pt$M_{0.05}$ electrocatalysts have markedly elevated dissolution resistance toward the state-of-the-art I^-/I_3^- redox electrolyte because of competitive reactions between *M* and I_2/I_3^- species. This study

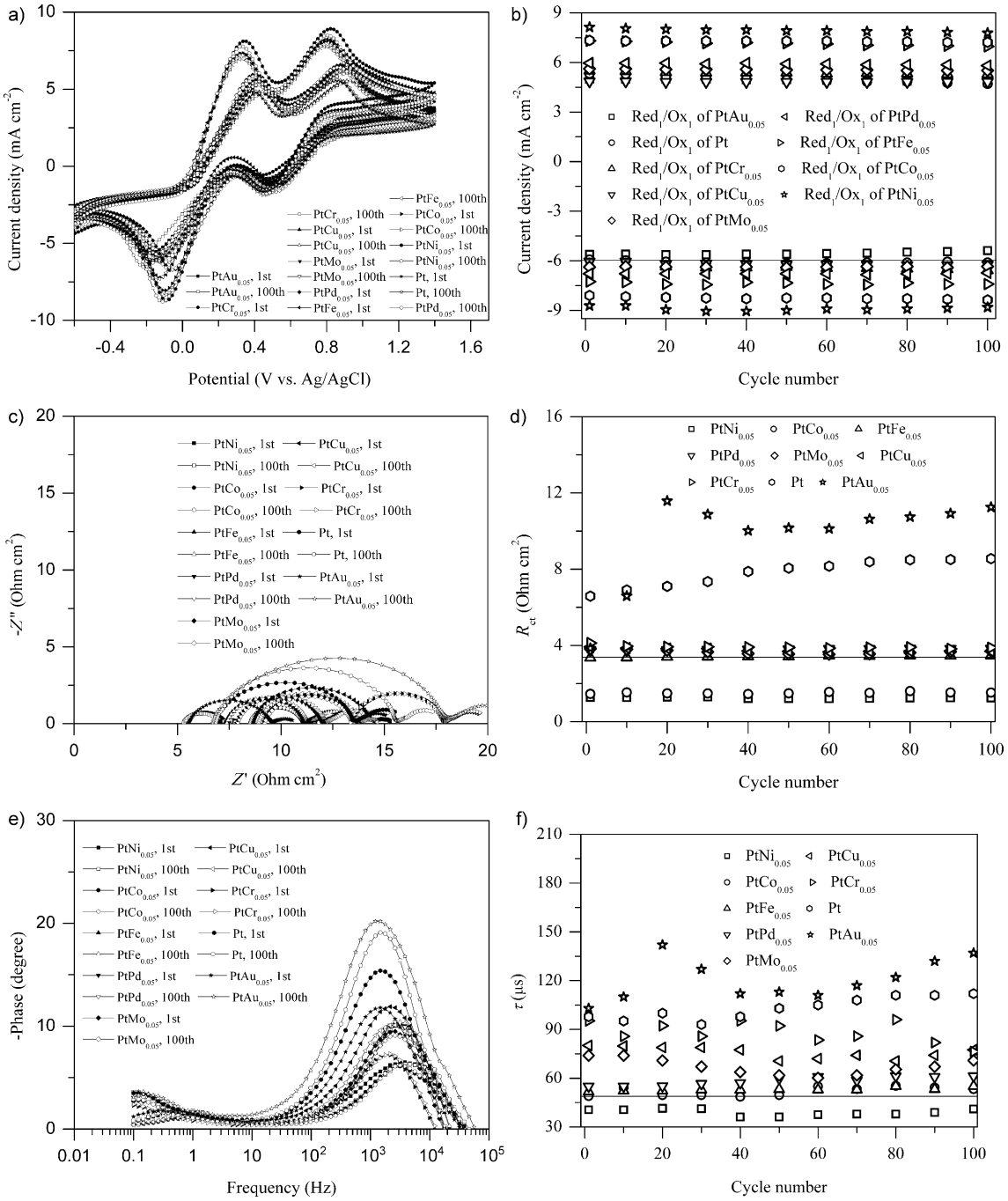

Figure 2. a) Repeated 100-cycle CV curves of the CEs in I^-/I_3^- redox electrolyte recorded at a scan rate of 50 mV s^{-1}. b) Plots of J_{Red1} and J_{Ox1} as a function of the cycle number. c) Repeated 100-cycle Nyquist and e) Bode EIS plots of the symmetric dummy cells from two identical CEs. Plots of d) R_{ct} and f) τ at the CE/electrolyte interface as a function of the cycle number.

presented here is far from being fully optimized, but these profound results suggest the launched strategy and Pt*M* alloy CEs holds great promise in developing stable and cost-effective DSSCs.

Acknowledgements

The authors acknowledge financial supports from Fundamental Research Funds for the Central Universities (grant number 201312005), National Key Technology Support Program (grant number 2012BAB15B02), and National High-Tech Research and Development Programme of China (grant numbers 2010AA09Z203, 2010AA065104).

Keywords: catalytic activity · counter electrodes · dissolution resistance · dye-sensitized solar cells · electrocatalysis

How to cite: *Angew. Chem. Int. Ed.* **2015**, *54*, 11448–11452
Angew. Chem. **2015**, *127*, 11610–11614

[1] B. O'Regan, M. Grätzel, *Nature* **1998**, *395*, 583–585.
[2] I. R. Perera, T. Daeneke, S. Makuta, Z. Yu, Y. Tachibana, A. Mishra, P. Bäuerle, C. A. Ohlin, U. Bach, L. Spiccia, *Angew. Chem. Int. Ed.* **2015**, *54*, 3758–3762; *Angew. Chem.* **2015**, *127*, 3829–3833.
[3] A. Hagfeldt, G. Boschloo, L. C. Sun, L. Kloo, H. Pettersson, *Chem. Rev.* **2010**, *110*, 6595–6663.
[4] N. Papageorgiou, W. F. Maier, M. Grätzel, *J. Electrochem. Soc.* **1997**, *144*, 876–884.
[5] S. Thomas, T. G. Deepak, G. S. Anjusree, T. A. Arun, S. V. Nair, S. Nair, *J. Mater. Chem. A* **2014**, *2*, 4474–4490.
[6] X. X. Chen, Q. W. Tang, B. L. He, L. Lin, L. M. Yu, *Angew. Chem. Int. Ed.* **2014**, *53*, 10799–10803; *Angew. Chem.* **2014**, *126*, 10975–10979.
[7] B. L. He, X. Meng, Q. W. Tang, *ACS Appl. Mater. Interfaces* **2014**, *6*, 4812–4818.
[8] Y. Y. Duan, Q. W. Tang, J. Liu, B. L. He, L. M. Yu, *Angew. Chem. Int. Ed.* **2014**, *53*, 14569–14574; *Angew. Chem.* **2014**, *126*, 14797–14802.
[9] X. J. Zheng, J. Deng, N. Wang, D. Deng, W. H. Zhang, X. H. Bao, C. Li, *Angew. Chem. Int. Ed.* **2014**, *53*, 7023–7027; *Angew. Chem.* **2014**, *126*, 7143–7147.
[10] J. W. Wan, G. Fang, H. Yin, X. Liu, D. Liu, M. Zhao, W. Ke, H. Tao, Z. Y. Tang, *Adv. Mater.* **2014**, *26*, 8101–8106.
[11] W. Chen, S. W. Chen, *J. Mater. Chem.* **2011**, *21*, 9169–9178.
[12] V. R. Stamenkovic, B. Fowler, B. S. Mun, G. Wang, P. N. Ross, C. A. Lucas, N. M. Marković, *Science* **2007**, *315*, 493–497.
[13] S. Zhang, X. Zhang, G. Jiang, H. Zhu, S. Guo, D. Su, G. Lu, S. Sun, *J. Am. Chem. Soc.* **2014**, *136*, 7734–7739.
[14] L. Su, S. Shrestha, Z. H. Zhang, W. Mustain, Y. Lei, *J. Mater. Chem. A* **2013**, *1*, 12293–12301.
[15] Z. B. Lv, J. F. Yu, H. W. Wu, J. Shang, D. Wang, S. C. Hou, Y. P. Fu, K. Wu, D. C. Zou, *Nanoscale* **2012**, *4*, 1248–1253.
[16] F. Calle-Vallejo, M. T. M. Koper, A. S. Bandarenka, *Chem. Soc. Rev.* **2013**, *42*, 5210–5230.
[17] M. K. Sabbe, L. Lain, M. F. Reyniers, G. B. Marin, *Phys. Chem. Chem. Phys.* **2013**, *15*, 12197–12214.
[18] I. Pašti, S. Mentus, *Phys. Chem. Chem. Phys.* **2009**, *11*, 6225–6233.

Received: June 11, 2015
Revised: June 27, 2015
Published online: July 21, 2015